INFLUENCE OF ILLUMINATION AND VIEWING CONDITIONS OF SOIL SURFACE ON REFLECTANCE CONTRAST BETWEEN ITS SOIL UNITS

JERZY CIERNIEWSKI
Adam Mickiewicz University, Institute of Physical Geography, Fredry 10, 61-701 Poznań, Poland

ABSTRACT

Using a geometrical model of soil bidirectional reflectance in the visible and near-infrared range, the reflectance contrast in changing illumination conditions was analyzed among typical soils of a diluvial plateau in the Wielkopolska Lowland situated in Western Poland. The model enabled a numerical determination of the influence of the solar zenith angle and the view zenith angle on the reflectance contrast between these soils. It also allowed the definition of the best zenith position of a sensor for the remote sensing interpretation of the analyzed soil cover for the changing zenith position of the Sun.

RÉSUMÉ

À l'aide d'un modèle géométrique de la réflexion à double sens du sol dans le spectre visible et proche-infrarouge, on a analysé le contraste de la réflexion dans les conditions changeantes d'illumination entre les sols typiques du plateau diluvial sur la plaine de Wielkopolska , située dans l'ouest de la Pologne. Le modèle a rendu possible la descripton numérique de l'influence de l'angle zénithal du Soleil et de l'angle zénithal de l'observation sur le contraste de la réflexion entre ces sols. Ce modèle a permis également de définir la meilleure position zénithale d'un capteur pour l'interpretation télédétective du couvert du sol analysé pour les positions changeantes du Soleil.

INTRODUCTION

Remotely sensed data on soil surfaces vary with soil moisture as well as the content and quality of soil pigments. In Central European conditions, they are mostly humus, iron oxides, and calcium carbonate. Soils, like many natural objects, also demonstrate non-Lambertian reflectance properties. Their brightness varies with the direction of irradiating solar energy and the direction along which the reflected energy is detected. The main reason of the non-Lambertian behaviour of soil surfaces is their irregularities, i.e., soil aggregates, clods and soil microrelief configurations, as elements casting shadows on these surfaces (Cierniewski, 1987, 1989; Cooper and Smith, 1985; Huete, 1987; Milton and Webb, 1987; Norman et al., 1985; Pech et al., 1986; Ransen et al., 1985). A soil seems to be brighter from a direction which displays a lower proportion of shaded fragments of its surface. Rough soil surfaces observed away from the Sun are usually brighter than when viewed towards the Sun. Soil surfaces with a higher roughness state display more variation in their brightness in their forward-and-backscattering viewing (Cierniewski and Courault, 1993; Cierniewski and Verbrugghe, 1994: Deering et al., 1990; Irons et al., 1992; Kimes and Seller, 1985). Thus, features of soil surface geometry, as well as the position of the Sun and the sensor determine the brightness of individual fragments of a soil cover recorded by remote sensing techniques. They are also responsible for the spectral contrast between adjoining soil fragments, making their separation in the image easier or more difficult.

Illumination and observation conditions which give a maximum contrast between soil units are analyzed in the paper. Typical soils of the Wielkopolska plain (western Poland) were selected for these studies. The contrast between the soils was numerically analyzed using a geometrical model of soil bidirectional reflectance, taking into account soil surface roughness parameters.

METHODS

The model

The model describes a soil surface as a structure composed of equal-sized opaque spheroids of horizontal (a) and vertical (b) radii, lying on a freely sloping (γ) plane. They are arranged on the surface in such a way that their centers in the horizontal projection are at a distance (d), irrespective of the azimuth position of their viewing. The structure is illuminated by sunbeams coming to its surface at the zenith angle (θs), and by diffuse skylight. The shaded and sunlit fragments of the given spheroid, the adjoining spheroids, and the ground surface between the spheroids, are observed within the field of view of the sensor. The position of border points between sunlit and shadowed fragments were found analytically by solving trigonometrical equations. The model assumes that slope angle (βi) of the sunlit soil surface fragments in relation to the angle of its azimuth position (ϕr), and angles of the sunbeams direction (θs, ϕs), determine wave energy reaching the sunlit fragments. The energy is determined, using the factor $E\beta i$, as:

$$E\beta i = \cos\theta s \cos\beta i + \sin\beta i \sin\theta s (\sin\phi s + \cos\phi s \cos\phi r).$$

The latest version of the model (Cierniewski et al., 1995) assumes that the energy leaving sunlit soil fragments is proportional to the energy coming to them and has specular-diffuse features. It means that the energy has not an isotropic distribution described by vectors creating a cloud of a circular shape like that of shaded fragments, but it disperses into many vectors creating an ellipsoidal cloud. Finally, the total relative radiance (L) of the simulated soil structure consisting of many (j) separate facets (i) is formulated as:

$$L = \frac{\sum_{i=1}^{j} (E\beta i \, Ii)(1 - f) + S f}{\sum_{i=1}^{j} Ii + S},$$

where Ii is the area of a directly illuminated facet (i), S is the area of a shaded fragment, and f is the ratio between the radiance of the shaded surface and the radiance of the same surface illuminated with sunbeams perpendicular to it.

Analyzed soils

The influence of soil surface roughness on the spectral contrast between the delineated soil units in their variable illumination and observation conditions was analyzed on the example of soils of the Kościan plain. They lie on a flat morainic plateau, stretching along the left bank of the Warta river to the north-west of Śrem at 16.88° E longitude and 52.14° N latitude. Typical soils of the plateau, i.e., the typical sols lessivés (Bt) occupying its highest, relatively flat fragments, the eroded sols lessivés (Be) with the argillic horizon on their surface developed on slopes of small local elevations, and the deluvial soils (Id) formed at the feet of the elevations, were selected for this analysis.

The soils were photographed from a height of 1.7 m on the background of a frame of 1 x 1 m size (Fig. 1). Their images were analyzed to characterize the roughness state of their surfaces. The soil surfaces were smoothed near the places where the photographs were taken. Then, they were viewed by a SPZ-02 field spectrophotometer constructed at the Space Research Centre in Warsaw. It is a 24-channel circular-variable filter instrument measuring reflectance energy in the range from 0.4 μm to 1.06 μm. The hemispherical-directional reflectance coefficient for each wavelength was determined by comparing the amount of energy reflected from the target with the amount of energy incident on the diffusing standard plate made of barium sulphate. All spectra were obtained vertically ($\theta v = 0°$) at a distance of 2.14 m from soil surfaces. The 15° field of view of the instrument integrated energy from an area of 0.25 m^2. The reflectance data were collected at the solar zenith angles (θs) of 44° to 46°.

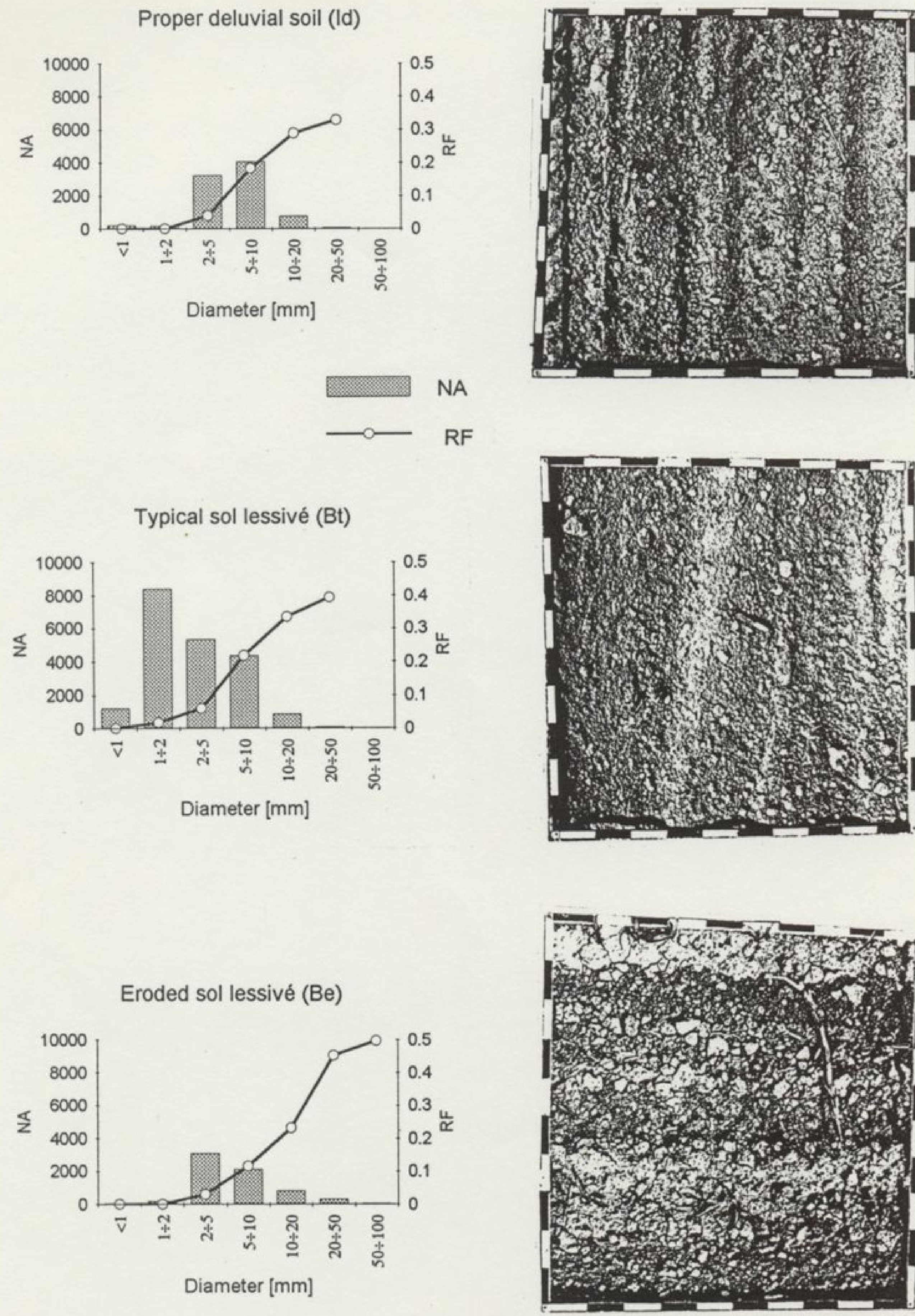

Fig. 1. Ground photographs of analized soil surfaces and their roughness parameters: NA - number of aggregates and clods in 1 m^2; RF - Sum of aggregates and clods area share of a given and a lower diameter.

The texture of the studied soils was determined by the aerometric method, while the organic matter content by loss-on-ignition when burned at 460°C. Their color in air-dry conditions was described using Munsell Color Charts.

RESULTS

Soil data representative of the analyzed soil units: their angle position on the slope, texture, and organic matter content, are presented in Table 1. Reflectance curves of the smoothed soils (Fig. 2) only characterize spectral features of the soil materials, eliminating the influence of their roughness state. The highest spectral contrast between them was found for the red wave of 0.744 μm length, corresponding with channel 19 of the spectrophotometer. Then, for that wavelength, using the above-mentioned soil bidirectional reflectance model, soil directional reflectance was simulated for three representative soil surfaces.

Table 1

Certain properties of studied soil surfaces

Ss	γ [°]	ϕr [°]	Mechanical fraction [mm] 2-0.05	0.05-0,002	<0,002	Texture	OM [%]	SC	RF
Id	2	185	89	10	1	sand	0,46	10YR6/4	0.328
Bt	1,5	185	77	20	3	loamy sand	1,59	10YR5/6	0.394
Be	3	105	69	18	13	sandy loam	2.90	10YR5/4	0.498

Ss - Soil symbol
γ - Slope angle
ϕr - Azimuth slope angle

MG - Mechanical group
OM - Organic matter content
SC - Soil color
RF - Roughness factor

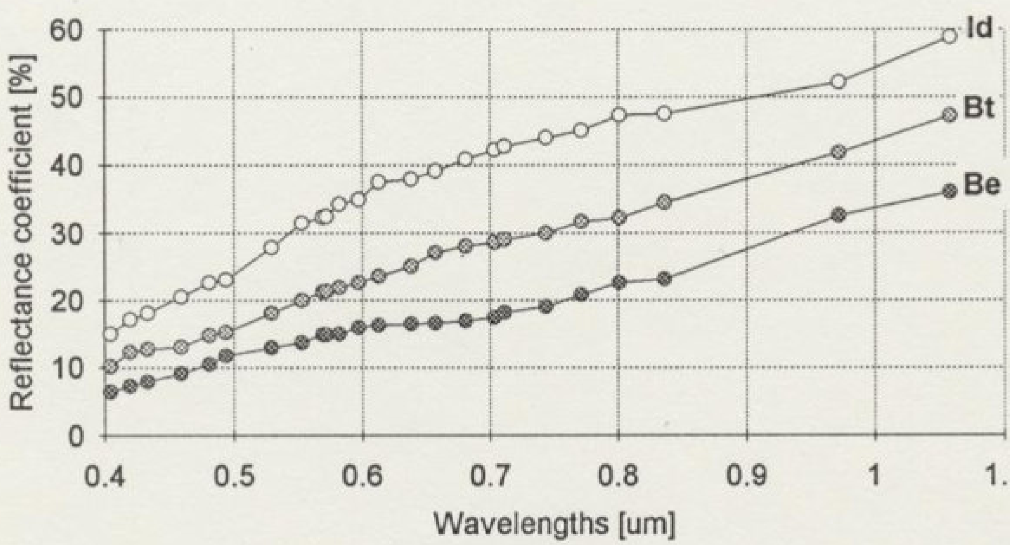

Fig. 2. Reflectance curves of smoothed surfaces of proper deluvial soil (Id), typical sol lessivé (Bt) and eroded sol lessivé (Be).

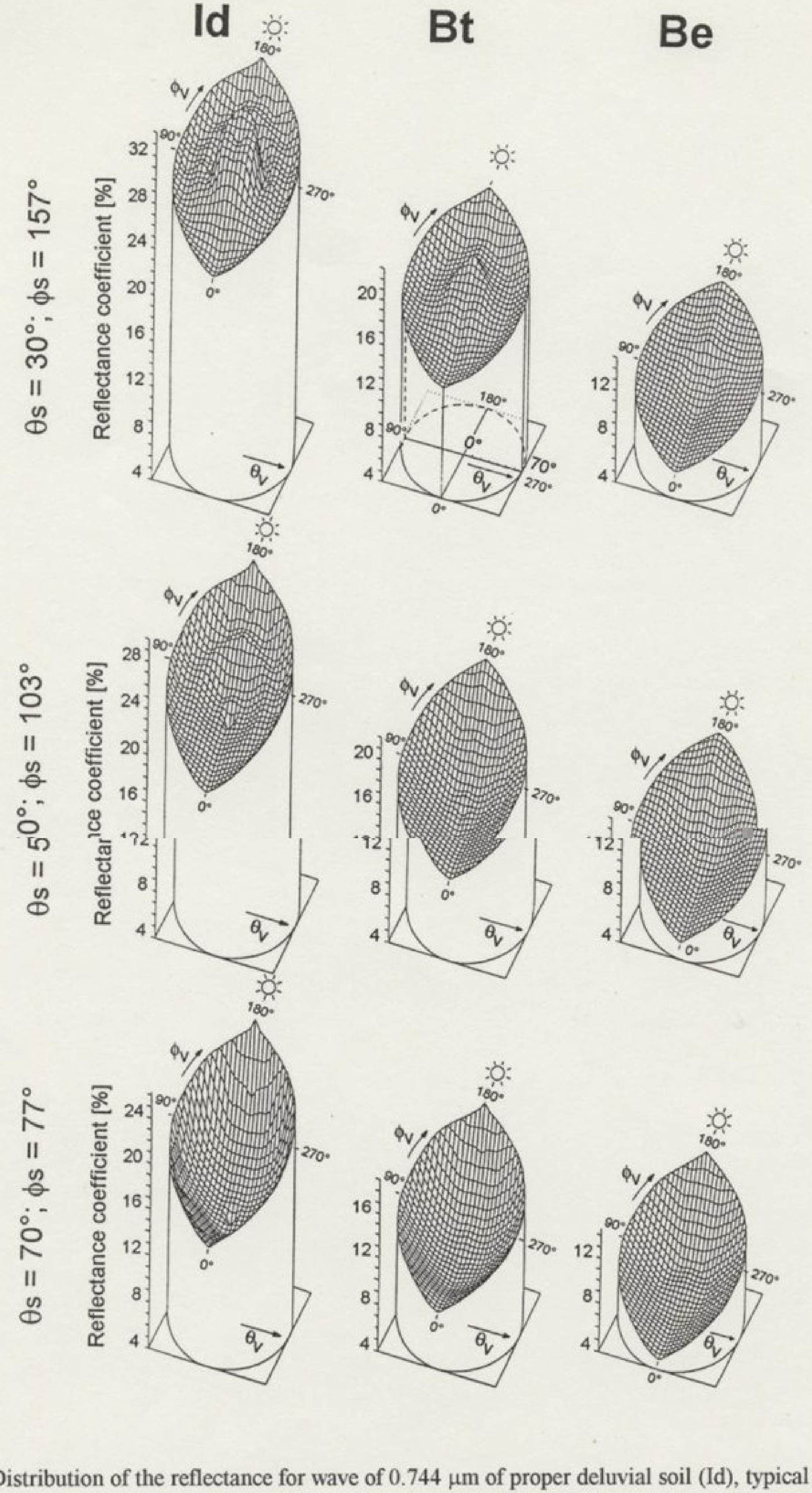

Fig. 3. Distribution of the reflectance for wave of 0.744 μm of proper deluvial soil (Id), typical sol lessivé (Bt) and eroded sol lessivé (Be) at different illumination conditions defined by solar zenith (θs) and azimuth (φs) angles and observation conditions described by zenithal (θv) and azimuthal (φv) angles.

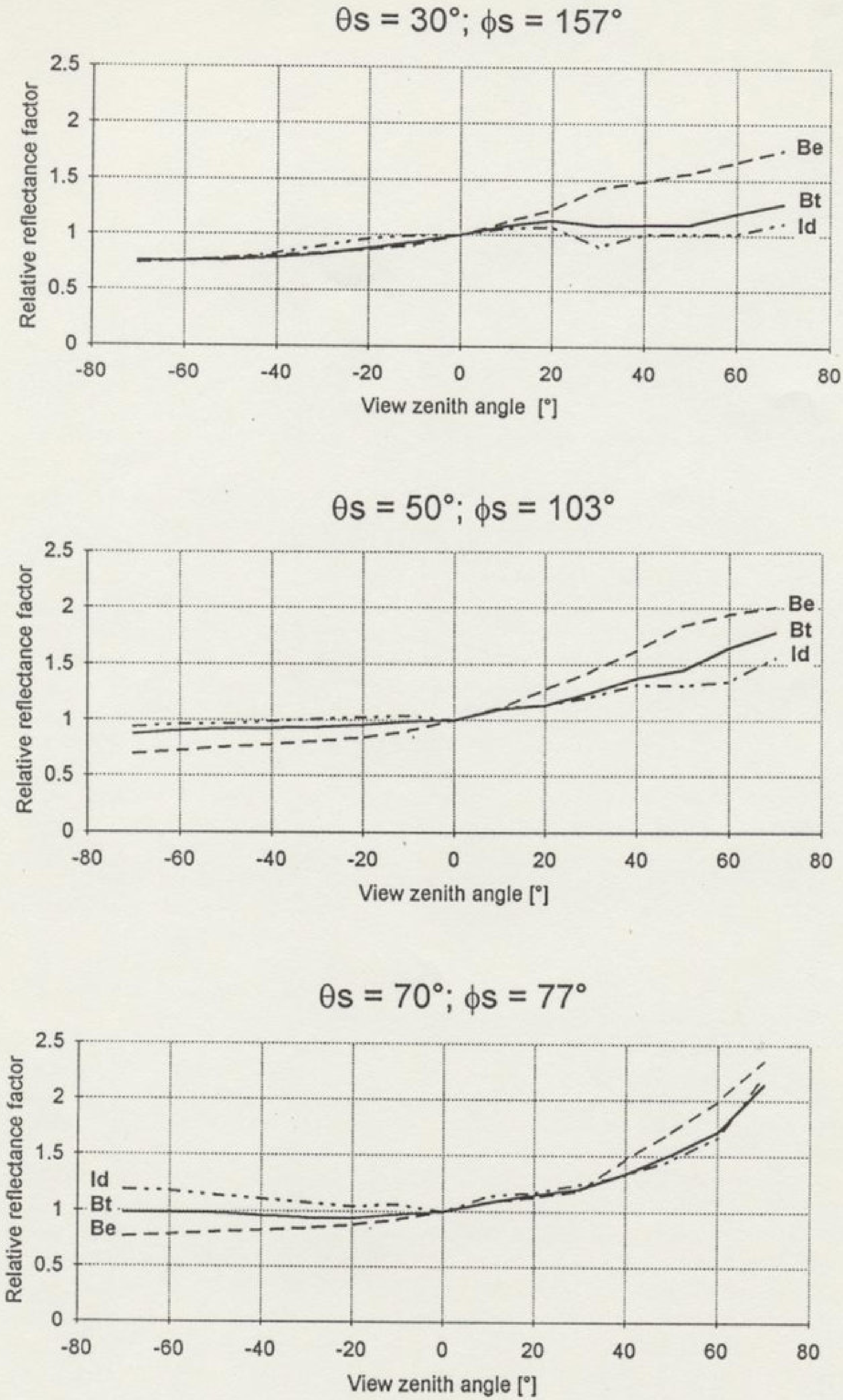

Fig. 4. Distribution of the relative reflectance factor for wave of 0.744 μm of proper deluvial soil (Id), typical sol lessivé (Bt) and eroded sol lessivé (Be) along the solar principle plane for selected illumination conditions defined by solar zenith (θs) and azimuth (φs). Negative values of the view zenith angle (θv) are forwardscatter and positive - backscatter.

The roughness state of the analyzed soil surfaces presented in Fig. 1 was defined in the model by two parameters: d/a and b/a. The first was calculated from the RF factor (Table 1), using the formula:

$$d/a = \sqrt{\pi / RF}.$$

The second was evaluated assuming the following values: 1, 2, and 0.75 for Bt, Be, and Id, respectively. The reflectance simulation was carried out for three zenith positions of the Sun (θs): 30°, 50°, and 70°. In order to make real the azimuth position of the Sun (ϕs), corresponding to their solar zenith angles (θs), the date of the simulation was set at 22th June. On the morning of that day, in the sample area defined by its geographical coordinates, zenith angles θs: 30°, 50°, and 70° correspond to ϕs angles: 157°, 103°, and 77°, respectively.

In the first step, the model simulated the distribution of the red wavelength along the solar plane, i.e., the plane azimuthally positioned like the Sun. The reflectance of the analyzed soil surfaces was calculated for view zenith angles (θv) in the range from 0° to 70° at 10° increments.

In the second step, the model generated the reflectance of the studied soils in the next six planes, azimuthally situated at a distance of 22.5° from one another. Diagrams in Fig. 3 show the reflectance of the soils with reference to the radiance of the standard barium sulphate plate. The reflectance is presented in the function of the view zenith (θv) and azimuth (ϕv) angles. Its variations for the analyzed soils for the same solar zenith angle result mainly from their different contents of organic matter and iron oxides. The reflectance decreases and the solar zenith angle (θs) increases as sunbeams become more and more horizontal. In turn, reflectance variation of the studied soil surfaces in the function of their view direction (θv and ϕv) depends primarily on their roughness state. The highest variation of reflectance resulting from roughness differences is obtained along the solar principal plane (ϕv=0° and ϕv=180°). Each of the analyzed soil surfaces is the brightest when viewed in the backscattering direction (ϕv=180°). Comparing the reflectance of the analyzed soils observed at a zenith angle (θv) equal to 70°, once viewed in the backscattering direction, and then in the forwardscattering one, the reflectance, if expressed in relation to the standard plate, varies by 10%, irrespective of the solar zenith angle. If the reflectance is expressed by the relative reflectance factor, i.e., as the ratio of soil radiance in the off-nadir direction to that in the nadir, we can observe other relationships (Fig. 4). The higher the soil surface roughness, the wider the variation of this factor in the solar principal plane. The relation is stronger for high solar zenith (θs) angles. If the θs is low, the variation is wider when a surface is viewed away from the Sun. Then, as the θs increases, the wider reflectance variation is observed towards the Sun. For θs angles higher than 60°, for relatively smooth soil surfaces, the effect of specular reflection appears in the forwardscattering range.

The goal of the studies was reached in the third step of the modelling, where the spectral contrast between the soils was calculated for each of the view directions. The model computed it between adjoining soils: proper deluvial soils and typical sols lessivés (Id - Bt), and also typical sols lessivés and eroded sols lessivés (Bt - Be) (Fig. 5). This contrast clearly grows as the solar zenith angle (θs) decreases. For the Id - Bt, observed in the nadir direction and illuminated at θs equal to 70°, 50°, and 30°, the model predicts the following contrast values: 3%, 7%, and 12.5%, respectively. For the Bt - Be in the same viewing and illumination conditions, it predicts the values 2.6%, 4.5%, and 9.4%, respectively. Looking at the soil units in the remaining analyzed directions, the model generated quite a different distribution of the contrast for the soil surfaces under these illumination conditions. For the high solar zenith angle, θs = 70°, the maximum contrast between the studied soils was observed in the backscattering directions. The higher the contrast, the higher the view zenith angle (θv) of the soils. When the Id - Bt is observed towards the Sun, the contrast between them grows only slightly with increasing θv, and for the Bt - Be it is nearly constant. This distribution of the contrast of the soils viewed towards the Sun is accounted for their specular reflectance, which is stronger for a low elevation of the Sun, and disappears as the solar zenith angle increases. For θs equal to 50° it is invisible, even along the solar principal plane. For the highest Sun elevation, θs = 30°, the maximum contrast between the studied soils becomes visible as a peak. It corresponds to view zenith angles lower than 30°, both in the backscattering and forwardscattering directions.

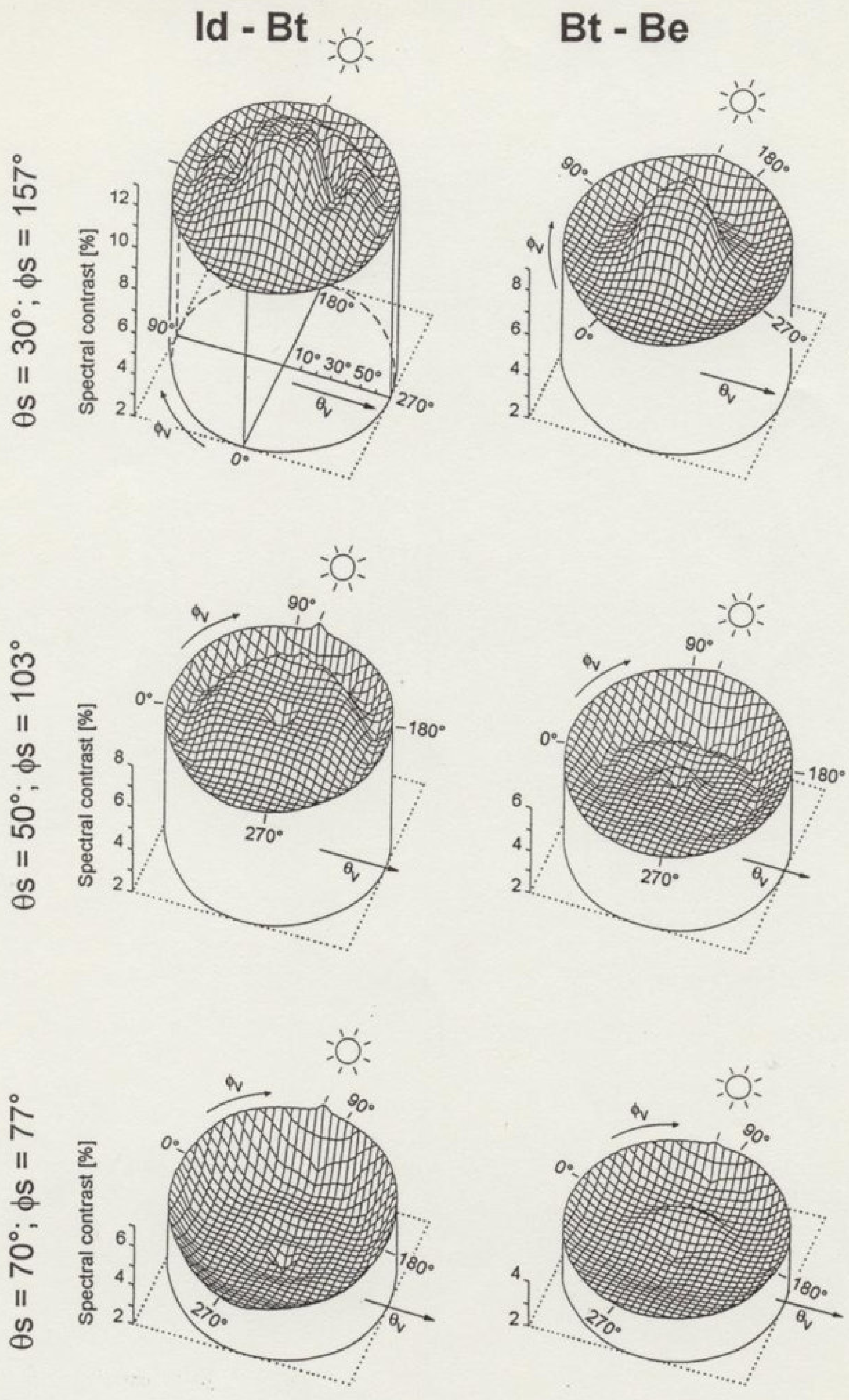

Fig. 5. Distribution of spectral contrast for wave of 0.744 μm between proper deluvial and typical sol lessivé (Id-Bt), and typical sol lessivé and eroded sol lessivé (Bt-Be) at a given illumination conditions defined by solar zenith (Θs) and azimuth (ϕs) angles for different view direction described by zenith (Θv) i azimuth (ϕv) angles.

CONCLUSIONS

While the analyzed soils: typical sols lessivés, eroded sols lessivés, and deluvial soils, are characterized by rather slight differences in their roughness states, they can vary widely in the spectral in the visible and near-infrared range depending on their illumination and observation conditions.

The maximum contrast between them is predicted for their illumination at possibly low solar zenith angles. If the angle is about 30°, the maximum contrast is expected for viewing them at zenith angles lower than 30°, both towards the Sun and away from it. If the solar zenith angle increases, the maximum contrast increases only in backscattering directions. The peak of the contrast, for low solar zenith angles and view zenith angles of similar values, disappears with a decrease in the Sun elevation, and the maximum becomes more and more visible at higher and higher view zenith angles.

REFERENCES

Cierniewski, J. (1987), A model for soil surface roughness influence on the spectral response of bare soils in the visible and near-infrared range, *Remote Sens. Environ.* 123: 97-115.

Cierniewski, J. (1989), The influence of the viewing geometry of bare rough soil surfaces on their spectral response in the visible and near-infrared range, *Remote Sens. Environ.* 127: 135-142.

Cierniewski, J. and Verbrugghe, M. (1994), A geometrical model of soil bidirectional reflectance in the visible and near-infrared range, *Proceedings of 6th International Measurements and Signatures in Remote Sensing, January 17-21 , 1994, Val d'Isere, France:* 635-642.

Cierniewski, J., Verbrugghe, M., Jacquemoud, S., Baret, F., and Hanocq, J. (1995), A geometrical modelling of soil bidirectional reflectance, to be published in *International Journal of Remote Sensing.*

Deering, D. W., Eack, T. F., and Otterman, J. (1990), Bidirectional reflectances of selected desert surfaces and their three-parameter soil characterization. *Agricultural and Forest Meteorology* 1, 52: 71-93.

Graetz, R. D. and Gentle, M. R. (1982), A study of the relationship between reflectance characteristics in the Landsat wavebands and the composition and structure of an Australian semi-arid rangeland, *Photogramm. Eng. Remote Sens.* 148: 1721-1736.

Huete, A. R. (1987), Soil and Sun angle interactions on partial canopy spectra, *Int. J. Remote Sens.* 18: 1307-1317.

Irons, J. R., Campbell, G. S., Norman, J. M., Graham, D., W., and Kovalick, W. M. (1992), Prediction and measurement of soil bidirectional reflectance, *IEEE Trans. Geosci Remote Sens.* 30, 2: 249-260.

Kimes, D. S., Seller, P. J. (1985), Inferring hemispherical reflectance of the Earth's surface for global energy budget from remotely sensed nadir or directional radiance values, *Remote Sens. Environ.* 118: 205-223.

Milton, E., J. and Webb, J., P. (1987), Ground radiometry and airborne, multispectral survey of bare soils, *Int. J. Remote Sens.* 18: 3-14.

Norman, J. M., Welles, J. M. and Walter, E. A. (1985), Contrast among bidirectional reflectance of leaves, canopies, and soils, *IEEE Trans. Geosci. Remote Sens.* 1GE-23: 659-667.

Pech, R. P., Graetz, R. R., Davis, A. W. (1986), Reflectance modelling and the derivation of vegetation indices for an Australian semi-arid shrubland. *Int. J. Remote Sens.* 17: 389-403.

Ranson, K. J., Biehl, L. L., and Bauer, M. E. (1985), Variation in spectral response of soybeans with respect to illumination, view and canopy geometry, *Int. J. Remote Sens.* 16: 1827-1842.